

Article

# Preferential CO Oxidation in H<sub>2</sub> over Au/La<sub>2</sub>O<sub>3</sub>/Al<sub>2</sub>O<sub>3</sub> Catalysts: The Effect of the Catalyst Reduction Method

Pandian Lakshmanan <sup>1,2</sup> and Eun Duck Park <sup>1,\*</sup>

<sup>1</sup> Department of Chemical Engineering and Department of Energy Systems Research, Ajou University, 206, World cup-ro, Yeongtong-Gu, Suwon 16499, Korea; lakshmanan.p@klu.ac.in

<sup>2</sup> Department of Chemistry, School of Advanced Sciences, Kalasalingam Academy of Research and Education, Krishnan koil, Tamil Nadu 626 126, India

\* Correspondence: edpark@ajou.ac.kr; Tel.: +82-31-219-2384

Received: 2 April 2018; Accepted: 18 April 2018; Published: 30 April 2018



**Abstract:** We investigated the influence of the reduction method on the preferential oxidation of CO in H<sub>2</sub> (CO-PROX) over Au/La<sub>2</sub>O<sub>3</sub>/Al<sub>2</sub>O<sub>3</sub> catalysts. An Au/La<sub>2</sub>O<sub>3</sub>/Al<sub>2</sub>O<sub>3</sub> sample, prepared using deposition–precipitation with urea, was reduced by chemical reduction with NaBH<sub>4</sub> or glycerol. Several techniques, such as diffuse-reflectance infrared Fourier-transform spectroscopy after CO adsorption (CO-DRIFTS), X-ray photoelectron spectroscopy (XPS) and transmission electron microscopy (TEM) were used to characterize the catalysts. Additionally, the catalysts were examined by in situ DRIFTS during methanol decomposition. The results reveal that the reduction method affects the average particle size and electronic state of gold, as well as the characteristics of the CO–Au<sup>0</sup> interactions. The best CO-PROX performance was observed for the catalyst chemically reduced using NaBH<sub>4</sub> with a NaBH<sub>4</sub>/Au molar ratio of 35. This catalyst contained gold particles with size of ~4 nm, for which the XPS binding energy was lower than that of metallic gold.

**Keywords:** gold; Au/La<sub>2</sub>O<sub>3</sub>/Al<sub>2</sub>O<sub>3</sub>; chemical reduction; NaBH<sub>4</sub>; glycerol; CO-PROX; effect of reduction method

## 1. Introduction

The catalytic removal of CO by preferential CO oxidation in H<sub>2</sub> (CO-PROX) is considered as a promising approach to prepare high-purity H<sub>2</sub> for polymer electrolyte membrane fuel cells [1]. Recent studies have revealed that gold can be an attractive alternative to platinum group metal (PGM)-based catalysts for this process [2], in view of its proven CO oxidation ability at low temperatures and lower catalytic performance in H<sub>2</sub>-mediated reactions [3–7]. In particular, the latter property derives from the lower capacity of gold to dissociate hydrogen compared with the PGM catalysts [8–10].

In order to improve the catalytic performance of gold centers in the CO-PROX process, much attention has been focused on the effects of the support and size of the gold particles. Previous investigations of the CO-PROX performance of nanosized gold catalysts supported on Al<sub>2</sub>O<sub>3</sub>-containing materials revealed that the support plays a more critical role [11–16] than the size of gold particles, because the rates of CO conversion and of undesirable H<sub>2</sub> oxidation increase as the gold particle size decreases and vice versa. The electronic state of gold nanoparticles depends on the nature of the support: slightly electron-deficient (Au<sup>δ+</sup>) or electron-rich (Au<sup>δ-</sup>) particles can be generated using acidic and basic oxides, respectively, due to the different charge transfer between the support and the gold particles [17,18]. In the case of Al<sub>2</sub>O<sub>3</sub>, which possesses both acidic and basic sites, positively and negatively charged metal nanoparticles can be formed [19]. The net charge on the gold nanoparticles can significantly influence the catalytic properties. Since the first report of favorable H<sub>2</sub> dissociation on Au<sup>0</sup> [20], basic oxide promoters such as lanthanum oxide have been found to be beneficial for the CO-PROX catalytic activity of gold supported on Al<sub>2</sub>O<sub>3</sub>-based oxides [11,21,22].

In the present study, the deposition–precipitation with urea (DPU) method was adopted to prepare Au/La<sub>2</sub>O<sub>3</sub>/Al<sub>2</sub>O<sub>3</sub> catalysts. In general, to obtain supported gold nanoparticles, the as-prepared sample is activated by thermal calcination and/or reduction. The thermal treatment, carried out under H<sub>2</sub> flow, results in the formation of smaller gold nanoparticles [23]. However, small gold particles are not favorable for all reactions, especially in the case of selective oxidations. Chemical reduction techniques have been employed to modify the characteristics of gold centers in supported catalysts [24]. The present study focuses on the effect of different reduction methods of the Au/La<sub>2</sub>O<sub>3</sub>/Al<sub>2</sub>O<sub>3</sub> catalyst on its CO-PROX activity. The activity of catalysts chemically reduced with aqueous NaBH<sub>4</sub> and pure glycerol was compared with that of their H<sub>2</sub>-reduced counterpart. The effects of the reduction method on the characteristics of the gold catalyst were studied by in situ diffuse-reflectance infrared Fourier-transform spectroscopy (DRIFTS) experiments, in which CO adsorption and methanol decomposition were carried out over the gold catalysts. In addition, transmission electron microscopy (TEM) and X-ray photoelectron spectroscopy (XPS) measurements were performed to inspect the changes in the properties of the gold catalyst according to the reduction method. The observed CO-PROX performance is discussed in light of the analyses mentioned above.

## 2. Results

### 2.1. CO-PROX Performance

The CO-PROX temperature profiles of the Au/La<sub>2</sub>O<sub>3</sub>/Al<sub>2</sub>O<sub>3</sub> catalysts reduced using different methods are shown in Figure 1. Interestingly, these profiles show considerable variation with the reduction method. The variation of the CO conversion with the reaction temperature reveals that the temperature of maximum CO conversion ( $T_{\max}$ ) is also considerably affected by the reduction method. The Au/La<sub>2</sub>O<sub>3</sub>/Al<sub>2</sub>O<sub>3</sub> (H) catalyst, reduced by the conventional thermal method under flowing hydrogen, exhibits the lowest  $T_{\max}$ , and achieves 97.6% CO conversion at 61 °C [22]. The  $T_{\max}$  value shifts to 95 °C (98.1% CO conversion) in the case of the Au/La<sub>2</sub>O<sub>3</sub>/Al<sub>2</sub>O<sub>3</sub> (S35) catalyst. Remarkably, the temperature window where high CO conversion is achieved is wider in the case of Au/La<sub>2</sub>O<sub>3</sub>/Al<sub>2</sub>O<sub>3</sub> (S35) as compared to Au/La<sub>2</sub>O<sub>3</sub>/Al<sub>2</sub>O<sub>3</sub> (H) (Table 1). These results highlight the favorable effects of chemical reduction with NaBH<sub>4</sub>. The maximum value of CO conversion and the drop in the CO conversion in CO-PROX at high temperatures are dependent on competition between H<sub>2</sub> and CO oxidation, which can be controlled by the catalyst design.

Motivated by the positive influence of NaBH<sub>4</sub> illustrated above, another aliquot of the as-prepared Au/La<sub>2</sub>O<sub>3</sub>/Al<sub>2</sub>O<sub>3</sub> sample was treated with a higher NaBH<sub>4</sub> concentration. This sample is denoted as Au/La<sub>2</sub>O<sub>3</sub>/Al<sub>2</sub>O<sub>3</sub> (S115). However, in this case the maximum CO conversion dropped dramatically, accompanied by a shift of  $T_{\max}$  towards high temperatures. The Au/La<sub>2</sub>O<sub>3</sub>/Al<sub>2</sub>O<sub>3</sub> (S5) catalyst, reduced with a very low concentration of NaBH<sub>4</sub>, exhibited similar catalytic performance to Au/La<sub>2</sub>O<sub>3</sub>/Al<sub>2</sub>O<sub>3</sub> (H) [22]. These results suggest that low and high concentrations of NaBH<sub>4</sub> are both ineffective for the chemical reduction of the catalyst.

A previous study revealed that an Au/CeO<sub>2</sub> catalyst reduced by glycerol showed higher activity for the selective oxidation of glycerol to lactic acid, as compared to the catalyst thermally reduced under flowing hydrogen [24]. This prompted us to apply the glycerol reduction method to the Au/La<sub>2</sub>O<sub>3</sub>/Al<sub>2</sub>O<sub>3</sub> catalyst. Figure 1 highlights the poor CO-PROX performance of the Au/La<sub>2</sub>O<sub>3</sub>/Al<sub>2</sub>O<sub>3</sub> (G) catalyst, as indicated by the high  $T_{\max}$  value. The O<sub>2</sub> conversion follows the same trend observed for the CO conversion (Figure 1). The chemically reduced samples exhibit slightly higher CO<sub>2</sub> selectivity compared with Au/La<sub>2</sub>O<sub>3</sub>/Al<sub>2</sub>O<sub>3</sub> (H) at low temperatures (Supplementary Information, Figure S1). The measured catalytic activities show that the CO-PROX temperature profile is sensitive to the catalyst reduction method. This could be attributed to the different characteristics of the gold nanoparticles formed in the different reduction processes.

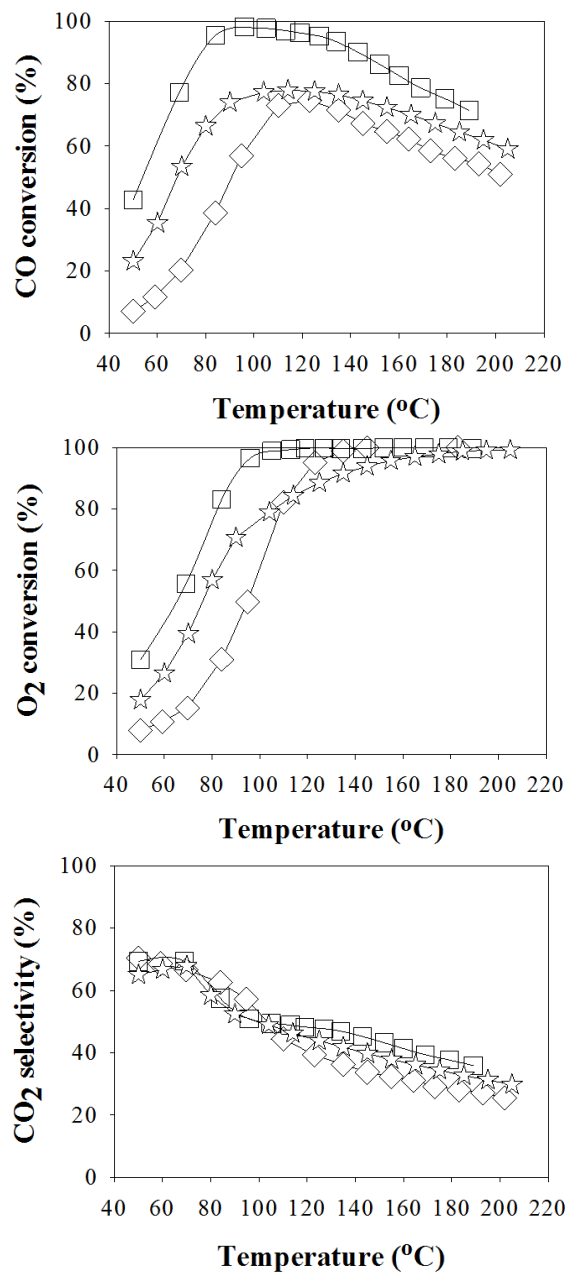


**Figure 1.** CO-PROX performance of Au/La<sub>2</sub>O<sub>3</sub>/Al<sub>2</sub>O<sub>3</sub> (S35) (□), Au/La<sub>2</sub>O<sub>3</sub>/Al<sub>2</sub>O<sub>3</sub> (S115) (☆), and Au/La<sub>2</sub>O<sub>3</sub>/Al<sub>2</sub>O<sub>3</sub> (G) (◇). Reaction conditions: 1 mol % CO, 1 mol % O<sub>2</sub>, 50 mol % H<sub>2</sub>, and 48 mol % He, F/W = 60,000 mL g<sub>cat</sub><sup>-1</sup> h<sup>-1</sup>. CO-PROX: preferential oxidation of CO in H<sub>2</sub>.

**Table 1.** Particle size of gold in Au/La<sub>2</sub>O<sub>3</sub>/Al<sub>2</sub>O<sub>3</sub> catalysts reduced under different conditions, and their CO-PROX activities.

Catalyst	Reducing Agents <sup>a</sup>	Average Particle Size of Gold (nm) <sup>b</sup>	Temperatures Achieving CO Conversions Higher than 97% (°C) <sup>c</sup>	Reference
Au/La <sub>2</sub> O <sub>3</sub> /Al <sub>2</sub> O <sub>3</sub> (H)	H <sub>2</sub>	2.9 ± 0.7	61	[22]
Au/La <sub>2</sub> O <sub>3</sub> /Al <sub>2</sub> O <sub>3</sub> (S5)	NaBH <sub>4</sub> (5) + H <sub>2</sub>	2.2 ± 0.2	61–74	[22]
Au/La <sub>2</sub> O <sub>3</sub> /Al <sub>2</sub> O <sub>3</sub> (S35)	NaBH <sub>4</sub> (35) + H <sub>2</sub>	4.2 ± 4.9	95–115	In this study
Au/La <sub>2</sub> O <sub>3</sub> /Al <sub>2</sub> O <sub>3</sub> (S115)	NaBH <sub>4</sub> (115) + H <sub>2</sub>	n.d.	-	In this study
Au/La <sub>2</sub> O <sub>3</sub> /Al <sub>2</sub> O <sub>3</sub> (G)	Glycerol + H <sub>2</sub>	3.0 ± 0.6	-	In this study

<sup>a</sup> The molar ratio of NaBH<sub>4</sub> to Au is included in parentheses; <sup>b</sup> The average particle size of gold was determined based on the TEM images; <sup>c</sup> The reaction conditions are same as those in Figure 1.

The NaBH<sub>4</sub>-reduced sample (without further reduction under flowing hydrogen) exhibited a maximum of 92% CO conversion at 91 °C (95.7% O<sub>2</sub> conversion and 48.2% selectivity to CO<sub>2</sub>) (Supplementary Information, Figure S2). The glycerol-reduced counterpart (without further reduction under flowing hydrogen) showed a maximum of 71% CO conversion at 155 °C. Without thermal treatment under H<sub>2</sub>, the catalytic results are inferior. The inferior performance compared to subsequent H<sub>2</sub>-reduced samples could be related mainly with incomplete reduction of gold. The effect of co-presence of H<sub>2</sub>O and CO<sub>2</sub> in the feed was tested with the Au/La<sub>2</sub>O<sub>3</sub>/Al<sub>2</sub>O<sub>3</sub> (S35) sample. A maximum of 93% CO conversion was observed at 97 °C (94.7% O<sub>2</sub> conversion and 49% selectivity to CO<sub>2</sub>) (Supplementary Information, Figure S3).

## 2.2. Characterization of the Catalysts

### 2.2.1. TEM Analysis

The TEM measurements show that the gold particle size distribution varies significantly with the reduction method (Figure 2). Only small gold particles ( $2.9 \pm 0.7$  nm) were observed for the Au/La<sub>2</sub>O<sub>3</sub>/Al<sub>2</sub>O<sub>3</sub> (H) catalyst [22]. On the other hand, comparatively larger gold particles ( $4.2 \pm 4.9$  nm) were found for the Au/La<sub>2</sub>O<sub>3</sub>/Al<sub>2</sub>O<sub>3</sub> (S35) sample (Figure 2a). The effect of the gold particle size is reflected in the CO-PROX temperature profiles. The higher  $T_{\max}$  measured for Au/La<sub>2</sub>O<sub>3</sub>/Al<sub>2</sub>O<sub>3</sub> (S35) compared to Au/La<sub>2</sub>O<sub>3</sub>/Al<sub>2</sub>O<sub>3</sub> (H) is consistent with the relatively larger Au particles in the S35 sample. The use of a higher concentration of NaBH<sub>4</sub> in the chemical reduction process resulted in large aggregates of gold particles in the Au/La<sub>2</sub>O<sub>3</sub>/Al<sub>2</sub>O<sub>3</sub> (S115) sample (Figure S4b). As a result, the maximum CO conversion showed a marked decrease. Chemical reduction with glycerol resulted in an average Au particle size of  $3.0 \pm 0.6$  nm for the Au/La<sub>2</sub>O<sub>3</sub>/Al<sub>2</sub>O<sub>3</sub> (G) catalyst (Figure 2b), which, however, exhibited the lowest catalytic performance. The TEM measurements thus reveal that the average Au particle size, and hence the catalytic performance, can be altered by using different methods to reduce the catalyst. The X-ray diffraction (XRD) patterns of the Al<sub>2</sub>O<sub>3</sub> and La<sub>2</sub>O<sub>3</sub>/Al<sub>2</sub>O<sub>3</sub> supports (Figure S5) reveal a substantial decrease in the intensity of the alumina peaks, owing to the presence of lanthanum oxide on the alumina surface. The characteristic XRD peaks of La<sub>2</sub>O<sub>3</sub> were not observed for La<sub>2</sub>O<sub>3</sub>/Al<sub>2</sub>O<sub>3</sub>, indicating that lanthanum oxide is present in an amorphous form on the alumina surface.

### 2.2.2. XPS Analysis

XPS measurements were performed in order to probe the effect of the catalyst reduction method on the characteristics of the resulting gold particles. The XPS spectra of Au/La<sub>2</sub>O<sub>3</sub>/Al<sub>2</sub>O<sub>3</sub> (H) exhibits Au 4f<sub>7/2</sub> and Au 4f<sub>5/2</sub> peaks at 83.8 and 87.4 eV, respectively (plot (a) in Figure 3), which are consistent with the binding energies of Au<sup>0</sup> [25–27]. All other samples exhibit binding energies shifted towards lower values compared to Au/La<sub>2</sub>O<sub>3</sub>/Al<sub>2</sub>O<sub>3</sub> (H). The Au 4f<sub>7/2</sub> binding energy in the Au/La<sub>2</sub>O<sub>3</sub>/Al<sub>2</sub>O<sub>3</sub> (S35) sample is shifted from 83.8 to 83.4 eV (plot (b) in Figure 3). The red shift in the binding energies of the chemically reduced samples indicates that the electronic properties of the gold nanoparticles in these samples differ significantly from those of the Au/La<sub>2</sub>O<sub>3</sub>/Al<sub>2</sub>O<sub>3</sub> (H) catalyst. The significant variation in the CO-PROX temperature profiles corresponding to different catalyst reduction methods can thus be attributed to the variation of characteristics of gold nanoparticles and variation of adsorption/reactivity of different gases in the reaction mixture.

### 2.2.3. CO-DRIFTS Measurements

In order to understand the effect of the catalyst reduction method, CO adsorption experiments at 80 °C were analyzed by in situ DRIFTS measurements. The evolution of the bands corresponding to CO adsorbed on Au particles was studied by recording the spectra at different time points during He purging. Figure 4a shows the evolution of the DRIFT spectra corresponding to Au/La<sub>2</sub>O<sub>3</sub>/Al<sub>2</sub>O<sub>3</sub> (H). We focus the analysis on the spectra measured after 3 min, which show the highest intensity in

Figure 4a. The band with the highest intensity, located at  $2107\text{ cm}^{-1}$ , is attributed to CO linearly adsorbed on low-coordinated Au sites [28–31], and is accompanied by a low-intensity shoulder centered at  $2025\text{ cm}^{-1}$ . The intensity of these bands decreases after 5 min and a new very weak band appears at  $1980\text{ cm}^{-1}$ . Thereafter, the intensity of all bands decreases with time. Boccuzzi et al. [32] reported bands corresponding to CO adsorbed on small Au clusters in the  $1950\text{--}2055\text{ cm}^{-1}$  range and attributed the band at  $1990\text{ cm}^{-1}$  to the stronger adsorption of CO on small Au clusters than on larger Au particles. Therefore, the bands observed at  $1980$  and  $2025\text{ cm}^{-1}$  can be attributed to CO strongly bonded to small gold clusters [26].

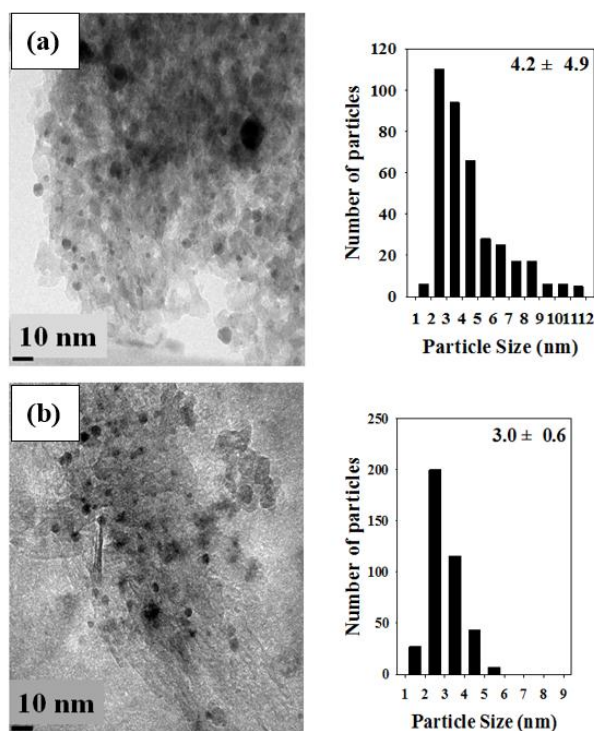


**Figure 2.** TEM images and gold size distributions of various Au/La<sub>2</sub>O<sub>3</sub>/Al<sub>2</sub>O<sub>3</sub> catalysts: (a) Au/La<sub>2</sub>O<sub>3</sub>/Al<sub>2</sub>O<sub>3</sub> (S35); (b) Au/La<sub>2</sub>O<sub>3</sub>/Al<sub>2</sub>O<sub>3</sub> (G).

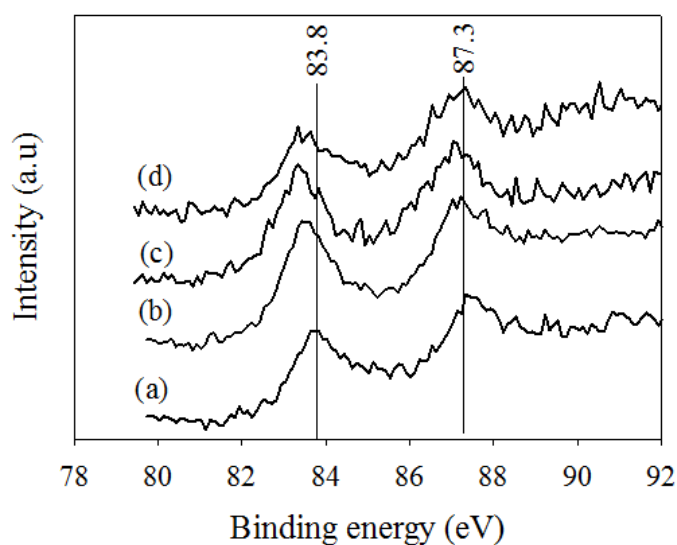


**Figure 3.** Au(4f) XP spectra of various Au/La<sub>2</sub>O<sub>3</sub>/Al<sub>2</sub>O<sub>3</sub> catalysts: (a) Au/La<sub>2</sub>O<sub>3</sub>/Al<sub>2</sub>O<sub>3</sub> (H); (b) Au/La<sub>2</sub>O<sub>3</sub>/Al<sub>2</sub>O<sub>3</sub> (S35); (c) Au/La<sub>2</sub>O<sub>3</sub>/Al<sub>2</sub>O<sub>3</sub> (S115); (d) Au/La<sub>2</sub>O<sub>3</sub>/Al<sub>2</sub>O<sub>3</sub> (G).

The evolution of the spectra of the Au/La<sub>2</sub>O<sub>3</sub>/Al<sub>2</sub>O<sub>3</sub> (S35) sample, obtained under identical conditions, is shown in Figure 4b. The band corresponding to CO linearly adsorbed on low-coordinated Au sites appears at 2112 cm<sup>-1</sup> after 3 min. The comparison of this spectrum with that measured at 3 min in Figure 4a reveals a clear blue shift of this band from 2107 to 2112 cm<sup>-1</sup>, due to the treatment with NaBH<sub>4</sub>. This blue shift indicates a stronger CO–Au<sup>0</sup> interaction [22], which is consistent with the highest CO conversion achieved by Au/La<sub>2</sub>O<sub>3</sub>/Al<sub>2</sub>O<sub>3</sub> (S35). The weak bands observed at 1980 and 2025 cm<sup>-1</sup> for Au/La<sub>2</sub>O<sub>3</sub>/Al<sub>2</sub>O<sub>3</sub> (H) (Figure 4a) are even less significant in the case of Au/La<sub>2</sub>O<sub>3</sub>/Al<sub>2</sub>O<sub>3</sub> (S35) (Figure 4b). This indicates that the contribution from CO species strongly bonded to small gold clusters is very small in this case. The TEM results (Table 1) further corroborate this conclusion: upon chemical reduction with NaBH<sub>4</sub>, the average gold size increases from 2.9 ± 0.7 to 4.2 ± 4.9 nm.

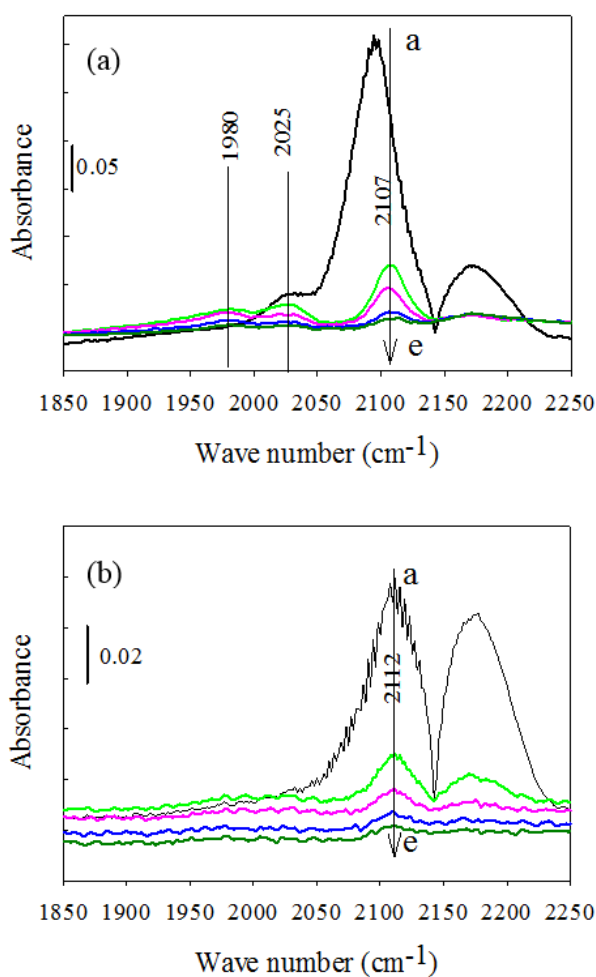


**Figure 4.** CO-DRIFT spectra of Au/La<sub>2</sub>O<sub>3</sub>/Al<sub>2</sub>O<sub>3</sub> catalysts: (a) Au/La<sub>2</sub>O<sub>3</sub>/Al<sub>2</sub>O<sub>3</sub> (H); (b) Au/La<sub>2</sub>O<sub>3</sub>/Al<sub>2</sub>O<sub>3</sub> (S35). Lines a to e correspond to spectra recorded after CO adsorption at 80 °C and subsequent He purge for 3, 5, 10, 20, and 30 min, respectively. CO-DRIFT: diffuse-reflectance infrared Fourier-transform spectroscopy after CO adsorption.

The time evolution of the spectra recorded during CO-DRIFTS measurements on Au/La<sub>2</sub>O<sub>3</sub>/Al<sub>2</sub>O<sub>3</sub> (S115) is presented in Figure 5a. The band attributed to CO linearly adsorbed on low-coordinated Au sites appears at 2114 cm<sup>-1</sup> after 3 min. The stronger blue shift of this band in Au/La<sub>2</sub>O<sub>3</sub>/Al<sub>2</sub>O<sub>3</sub> (S115) than in Au/La<sub>2</sub>O<sub>3</sub>/Al<sub>2</sub>O<sub>3</sub> (S35) (Figure 4b) could be attributed to the higher concentration of sodium borohydride employed for the chemical reduction process.

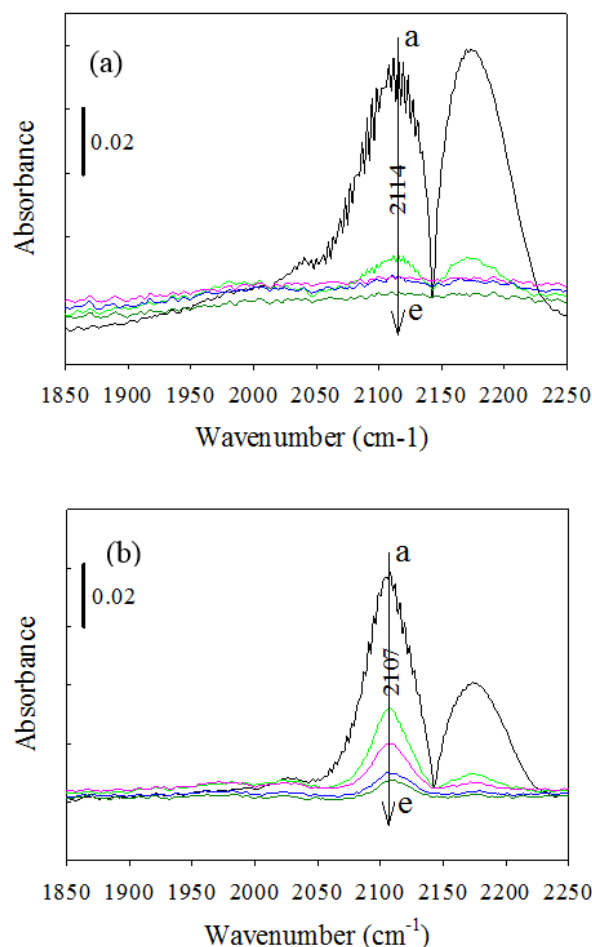


**Figure 5.** CO-DRIFT spectra of Au/La<sub>2</sub>O<sub>3</sub>/Al<sub>2</sub>O<sub>3</sub> catalysts: (a) Au/La<sub>2</sub>O<sub>3</sub>/Al<sub>2</sub>O<sub>3</sub> (S115); (b) Au/La<sub>2</sub>O<sub>3</sub>/Al<sub>2</sub>O<sub>3</sub> (G). Lines a to e correspond to spectra recorded after CO adsorption at 80 °C and subsequent He purge for 3, 5, 10, 20, and 30 min, respectively.

The comparison of the spectra measured at 10, 20, and 30 min in Figures 4b and 5a highlights a sharp decrease in the intensities of these bands for Au/La<sub>2</sub>O<sub>3</sub>/Al<sub>2</sub>O<sub>3</sub> (S115). These results suggest that the amount of chemisorbed CO decreases when higher concentrations of NaBH<sub>4</sub> are used for the catalyst reduction. This explains the low CO-PROX performance of Au/La<sub>2</sub>O<sub>3</sub>/Al<sub>2</sub>O<sub>3</sub> (S115) (Figure 1) and is consistent with the presence of large aggregates of gold particles, as observed in the TEM images (Figure S4b). Figure 5b shows the time evolution of the spectra recorded during CO-DRIFTS measurements for Au/La<sub>2</sub>O<sub>3</sub>/Al<sub>2</sub>O<sub>3</sub> (G). The band corresponding to CO linearly adsorbed on low-coordinated Au sites is observed at 2107 cm<sup>-1</sup> after 3 min. The comparison between Figures 4a and 5b reveals a large difference in the intensity of the shoulder peak centered at 2025 cm<sup>-1</sup>. This band corresponds to CO strongly bonded to small gold clusters [26]. Such contribution is negligible in the case of Au/La<sub>2</sub>O<sub>3</sub>/Al<sub>2</sub>O<sub>3</sub> (G), in agreement with its low CO conversion (Figure 1).

#### 2.2.4. DRIFTS Analysis during Methanol Decomposition

To assess the effect of the reduction method on the catalytic activity of the gold particles, the reactivity of adsorbed methanol was investigated by in situ DRIFTS. Methanol adsorption experiments were performed at 160 °C and the spectra were collected after subsequent He purging for 5 min (Figures 6–8). Several bands located in the 1018–1100 cm<sup>-1</sup> range (Figure 6) can be attributed to different methoxy species [33–36]. The bands centered at 1033 and 1056 cm<sup>-1</sup> exhibit the highest intensity in the case of Au/La<sub>2</sub>O<sub>3</sub>/Al<sub>2</sub>O<sub>3</sub> (S35) (plot (c) in Figure 6), indicative of enhanced methanol

adsorption on this catalyst. The adsorbed methoxy species undergoes further transformation into formate species.

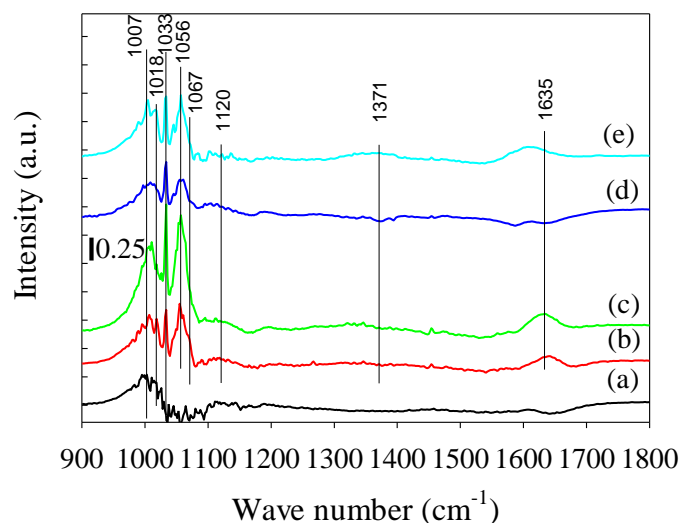


**Figure 6.** In situ DRIFT spectra of Au/La<sub>2</sub>O<sub>3</sub>/Al<sub>2</sub>O<sub>3</sub> catalysts after methanol adsorption at 160 °C and subsequent He purge for 5 min: (a) La<sub>2</sub>O<sub>3</sub>/Al<sub>2</sub>O<sub>3</sub>; (b) Au/La<sub>2</sub>O<sub>3</sub>/Al<sub>2</sub>O<sub>3</sub> (H); (c) Au/La<sub>2</sub>O<sub>3</sub>/Al<sub>2</sub>O<sub>3</sub> (S35); (d) Au/La<sub>2</sub>O<sub>3</sub>/Al<sub>2</sub>O<sub>3</sub> (S115); (e) Au/La<sub>2</sub>O<sub>3</sub>/Al<sub>2</sub>O<sub>3</sub> (G).

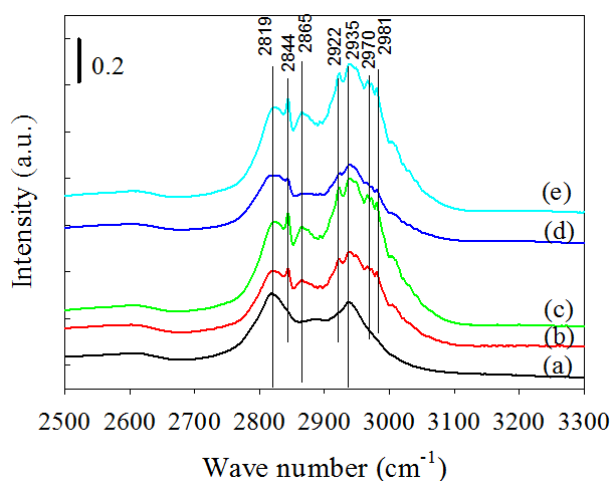


**Figure 7.** In situ DRIFT spectra of Au/La<sub>2</sub>O<sub>3</sub>/Al<sub>2</sub>O<sub>3</sub> catalysts after methanol adsorption at 160 °C and subsequent He purge for 5 min: (a) La<sub>2</sub>O<sub>3</sub>/Al<sub>2</sub>O<sub>3</sub>; (b) Au/La<sub>2</sub>O<sub>3</sub>/Al<sub>2</sub>O<sub>3</sub> (H); (c) Au/La<sub>2</sub>O<sub>3</sub>/Al<sub>2</sub>O<sub>3</sub> (S35); (d) Au/La<sub>2</sub>O<sub>3</sub>/Al<sub>2</sub>O<sub>3</sub> (S115); (e) Au/La<sub>2</sub>O<sub>3</sub>/Al<sub>2</sub>O<sub>3</sub> (G).

The bands observed around 1371 and 1635 cm<sup>-1</sup> can be attributed to the  $\nu_s$  (OCO) and  $\nu_a$  (OCO) stretching modes of formate species, respectively (Figure 6) [33,34]. Note that the intensity of the band at 1635 cm<sup>-1</sup> is relatively high for Au/La<sub>2</sub>O<sub>3</sub>/Al<sub>2</sub>O<sub>3</sub> (S35). The transformation of methoxy to formate is slightly more effective over Au/La<sub>2</sub>O<sub>3</sub>/Al<sub>2</sub>O<sub>3</sub> (S35) than Au/La<sub>2</sub>O<sub>3</sub>/Al<sub>2</sub>O<sub>3</sub> (H). The symmetric stretching modes of the methoxy CH bond,  $\nu_s$  (C–H) and  $\nu_a$ (C–H), have been reported in the 2819–2859 cm<sup>-1</sup> and 2920–2960 cm<sup>-1</sup> ranges, respectively [33,34]. The bands observed at 2844, 2865, 2922, 2935, 2970, and 2981 cm<sup>-1</sup> in Figure 7 could be attributed to the CH bond of formate species [33,34]. In particular, compared with Au/La<sub>2</sub>O<sub>3</sub>/Al<sub>2</sub>O<sub>3</sub> (H) (plot (b) in Figure 7), these bands show higher intensity for Au/La<sub>2</sub>O<sub>3</sub>/Al<sub>2</sub>O<sub>3</sub> (S35) (plot (c) in Figure 7), whereas their intensity is weaker in the case of Au/La<sub>2</sub>O<sub>3</sub>/Al<sub>2</sub>O<sub>3</sub> (S115) (plot (d) in Figure 7).

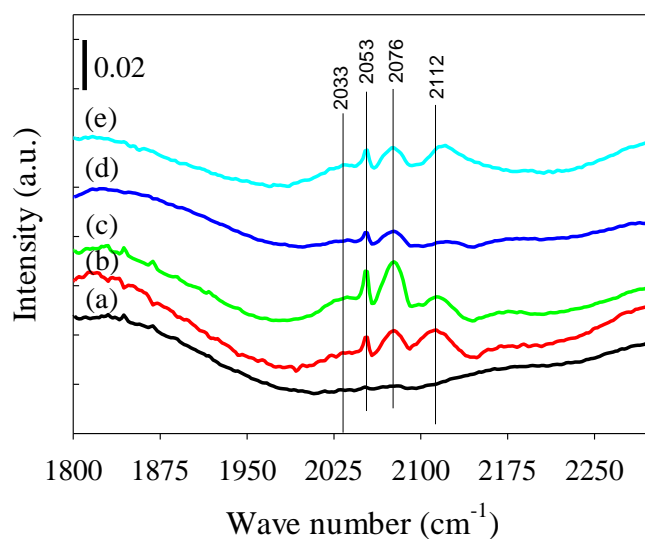


**Figure 8.** In situ DRIFT spectra of Au/La<sub>2</sub>O<sub>3</sub>/Al<sub>2</sub>O<sub>3</sub> catalysts after methanol adsorption at 160 °C and subsequent He purge for 5 min: (a) La<sub>2</sub>O<sub>3</sub>/Al<sub>2</sub>O<sub>3</sub>; (b) Au/La<sub>2</sub>O<sub>3</sub>/Al<sub>2</sub>O<sub>3</sub> (H); (c) Au/La<sub>2</sub>O<sub>3</sub>/Al<sub>2</sub>O<sub>3</sub> (S35); (d) Au/La<sub>2</sub>O<sub>3</sub>/Al<sub>2</sub>O<sub>3</sub> (S115); (e) Au/La<sub>2</sub>O<sub>3</sub>/Al<sub>2</sub>O<sub>3</sub> (G).

CO is formed upon further transformation of formate species on the gold catalyst. Figure 8 shows the variation in the intensity of the peak corresponding to CO adsorbed on gold (formed via methanol decomposition) among the different catalysts. In general, four bands could be observed for all samples. The band around 2112 cm<sup>-1</sup> corresponds to linear CO adsorbed on Au<sup>0</sup> particles [28,32]. The bands centered at 2053 [29,37] and 2076 cm<sup>-1</sup> [38] have been attributed to CO adsorbed on negatively charged gold clusters (Au<sup>δ-</sup>-CO species), formed upon electron transfer from the support to the gold clusters [29,32,37,38]. Finally, the band at 2033 cm<sup>-1</sup> corresponds to bridge-bonded CO species on small gold clusters [32]. As expected, these bands were not observed for La<sub>2</sub>O<sub>3</sub>/Al<sub>2</sub>O<sub>3</sub> (plot (a) in Figure 8). Au/La<sub>2</sub>O<sub>3</sub>/Al<sub>2</sub>O<sub>3</sub> (S35) (plot (c) in Figure 8) exhibits the highest intensity of the band centered at 2076 cm<sup>-1</sup>, which corresponds to CO adsorbed on negatively charged Au<sup>δ-</sup> sites [32,37]. A similar observation can also be made for the band at 2053 cm<sup>-1</sup>. The higher intensity of the band corresponding to CO adsorbed on negatively charged Au<sup>δ-</sup> sites [32,37] in the case of Au/La<sub>2</sub>O<sub>3</sub>/Al<sub>2</sub>O<sub>3</sub> (S35) could be attributed to the chemical reduction with NaBH<sub>4</sub>. Note the Au 4f<sub>7/2</sub> binding energy shift from 83.8 to 83.4 eV in Au/La<sub>2</sub>O<sub>3</sub>/Al<sub>2</sub>O<sub>3</sub> (S35), relative to that of Au/La<sub>2</sub>O<sub>3</sub>/Al<sub>2</sub>O<sub>3</sub> (H). This supports the presence of negatively charged Au<sup>δ-</sup> sites in Au/La<sub>2</sub>O<sub>3</sub>/Al<sub>2</sub>O<sub>3</sub> (S35). The high-intensity bands in the DRIFTS spectra of methanol-derived CO (Figure 8) measured for Au/La<sub>2</sub>O<sub>3</sub>/Al<sub>2</sub>O<sub>3</sub> (S35) indicate a higher reactivity of adsorbed methanol on this catalyst with respect to the other samples. The highest CO conversion obtained with Au/La<sub>2</sub>O<sub>3</sub>/Al<sub>2</sub>O<sub>3</sub> (S35) in the CO-PROX temperature profiles (Figure 1 and Table 1) is in line with the results of the DRIFTS measurements during methanol decomposition. As could be noted from the Figure 1, the selectivity to CO<sub>2</sub> varies with the catalyst reduction method. The interactions of oxygen and hydrogen with gold particles are also very important to explain the activity of gold catalysts towards the CO-PROX reaction. Due to increased competition between CO and H<sub>2</sub> oxidation, the selectivity of CO<sub>2</sub> decreases with temperature. Moreover, the very weak intensity of the band at 2112 cm<sup>-1</sup> for Au/La<sub>2</sub>O<sub>3</sub>/Al<sub>2</sub>O<sub>3</sub> (S115) (plot (d) in Figure 8), as compared with the other samples, suggests a very low reactivity of methanol adsorbed on Au<sup>0</sup> particles for this catalyst. The band at 2033 cm<sup>-1</sup>, corresponding to the bridge-bonded CO species on small gold clusters [32], is also absent for this catalyst (plot (d) in Figure 8). This is in line with the TEM results, which revealed the presence of large aggregates of gold particles in this sample. Finally, Au/La<sub>2</sub>O<sub>3</sub>/Al<sub>2</sub>O<sub>3</sub> (G) exhibits weaker bands at 2033, 2053, and 2076 cm<sup>-1</sup>, as compared with Au/La<sub>2</sub>O<sub>3</sub>/Al<sub>2</sub>O<sub>3</sub> (S35).

To summarize the insight obtained from the DRIFTS analysis of methanol-derived CO, Au/La<sub>2</sub>O<sub>3</sub>/Al<sub>2</sub>O<sub>3</sub> (S35) exhibits stronger bands corresponding to methoxy/formate species and

methanol-derived CO compared with Au/La<sub>2</sub>O<sub>3</sub>/Al<sub>2</sub>O<sub>3</sub> (H). The band centered at 2076 cm<sup>-1</sup>, assigned to CO adsorbed on negatively charged Au<sup>δ-</sup> sites, also exhibits the highest intensity in the case of Au/La<sub>2</sub>O<sub>3</sub>/Al<sub>2</sub>O<sub>3</sub> (S35) (plot (c) in Figure 8). Trueba et al. [19] and Boronat et al. [20] showed that negatively charged gold sites can favor CO oxidation by suppressing hydrogen conversion. In the normal CO-DRIFTS experiments, the band corresponding to CO linearly adsorbed on low-coordinated Au sites exhibits a blue shift from 2107 cm<sup>-1</sup> (Figure 4a) to 2112 cm<sup>-1</sup> (Figure 4b), indicating stronger CO–Au<sup>0</sup> interactions in the case of Au/La<sub>2</sub>O<sub>3</sub>/Al<sub>2</sub>O<sub>3</sub> (S35). These results are in agreement with the DRIFTS spectra of methanol-derived CO. The Au/La<sub>2</sub>O<sub>3</sub>/Al<sub>2</sub>O<sub>3</sub> (S35) sample exhibits the highest CO conversion in the CO-PROX experiments, which further corroborates the conclusions of the DRIFTS analysis. In addition to small clusters, medium and relatively large gold particles co-exist, as revealed by methanol-derived CO-DRIFTS. Therefore, the distribution of such gold particles among different samples cannot be ignored in the comparison of catalytic results.

### 3. Discussion

Interestingly, while the band at 2076 cm<sup>-1</sup> is merged with the main band centered at 2107 cm<sup>-1</sup> in the CO-DRIFTS spectra (Figures 4 and 5), the two bands are clearly separated in the DRIFTS spectra of methanol-derived CO (Figure 8). It can thus be concluded that the DRIFTS analysis of methanol-derived CO can be more informative than that of normal CO.

The comparison of plots (c) and (d) in Figure 6 highlights a lower intensity of the bands corresponding to adsorbed methoxy species (1033 and 1056 cm<sup>-1</sup>) in the latter case. A similar trend is observed for the bands corresponding to formate and methanol-derived CO (compare plots (c) and (d) in Figures 7 and 8). These results show that higher concentrations of NaBH<sub>4</sub> lead to a decrease in the reactivity of methanol over Au/La<sub>2</sub>O<sub>3</sub>/Al<sub>2</sub>O<sub>3</sub> (S115). This is consistent with the inferior CO-PROX performance of Au/La<sub>2</sub>O<sub>3</sub>/Al<sub>2</sub>O<sub>3</sub> (S115). Moreover, a low concentration of NaBH<sub>4</sub> is also ineffective in the case of Au/La<sub>2</sub>O<sub>3</sub>/Al<sub>2</sub>O<sub>3</sub> (S5) (Table 1). Therefore, it can be concluded that the concentration of NaBH<sub>4</sub> used in the chemical reduction process must be optimized. Chemical reduction with glycerol does not appear to have a positive influence on the reactivity of adsorbed methanol (plot (e) in Figure 6). A similar conclusion can be drawn for the CO-PROX experiments. The FTIR analysis (Figure S6) shows the presence of bands related to glycerol and glycerol-derived intermediates [39–43], due to incomplete removal of glycerol from the catalyst surface, which resulted in the poor CO-PROX performance.

## 4. Materials and Methods

### 4.1. Preparation of Catalysts

The La<sub>2</sub>O<sub>3</sub>/Al<sub>2</sub>O<sub>3</sub> support was prepared using the wet impregnation method [22]. An appropriate amount of La(NO<sub>3</sub>)<sub>3</sub>·6H<sub>2</sub>O (≥99.9%, Sigma-Aldrich, St. Louis, MO, USA) was dissolved in ethanol (99.5%, Sigma-Aldrich, St. Louis, MO, USA) at room temperature, followed by addition of Al<sub>2</sub>O<sub>3</sub> (Alfa Aesar, Brunauer-Emmett-Teller surface area, S<sub>BET</sub> = 150 m<sup>2</sup> g<sup>-1</sup>) and vigorous stirring for 1 h at room temperature. Ethanol was gradually removed with a rotary evaporator at 60 °C. The obtained powder was subsequently dried in an oven at 100 °C for 12 h and finally calcined in air at 500 °C for 5 h. Gold was loaded on the calcined La<sub>2</sub>O<sub>3</sub>/Al<sub>2</sub>O<sub>3</sub> support using the DPU method (Supplementary Information).

The as-prepared Au/La<sub>2</sub>O<sub>3</sub>/Al<sub>2</sub>O<sub>3</sub> sample was reduced by conventional thermal methods under flowing hydrogen at 200 °C for 2 h, and the product was denoted Au/La<sub>2</sub>O<sub>3</sub>/Al<sub>2</sub>O<sub>3</sub> (H). Aliquots of the as-prepared sample were chemically reduced by different methods prior to thermal reduction with H<sub>2</sub> at 200 °C. The as-prepared sample was reduced with aqueous NaBH<sub>4</sub> at 25 °C. In a typical chemical reduction process, 0.150 g of the finely powdered as-prepared sample was mixed with deionized water and stirred vigorously for 30 min. Subsequently, an aqueous solution of NaBH<sub>4</sub> (with variable concentrations) was slowly added dropwise, followed by vigorous stirring at ambient temperature for 30 min. The reduction of gold was followed by an immediate color change from yellow to brown.

Excess water was removed by centrifugation. The obtained sample was thoroughly washed with deionized water several times and subsequently dried under a vacuum.

Chemical reduction was performed with different  $\text{NaBH}_4/\text{Au}$  molar ratios (5, 35, and 115). All samples were further reduced under flowing  $\text{H}_2$  at 200 °C for 2 h, prior to the CO-PROX reaction. The products corresponding to  $\text{NaBH}_4/\text{Au}$  molar ratios of 5, 35, and 115 are denoted  $\text{Au}/\text{La}_2\text{O}_3/\text{Al}_2\text{O}_3$  (S5),  $\text{Au}/\text{La}_2\text{O}_3/\text{Al}_2\text{O}_3$  (S35), and  $\text{Au}/\text{La}_2\text{O}_3/\text{Al}_2\text{O}_3$  (S115). Another portion of the as-prepared  $\text{Au}/\text{La}_2\text{O}_3/\text{Al}_2\text{O}_3$  sample was used for chemical reduction with glycerol (CRG) [24] (Supplementary Information).

#### 4.2. Characterization of Catalysts

The physicochemical properties of the prepared catalysts were probed with a variety of characterization techniques such as  $\text{N}_2$  physisorption, powder X-ray diffraction (XRD), inductively coupled plasma atomic emission spectroscopy ICP-AES, TEM, DRIFTS, and XPS. The detailed procedure for each experiment is described in the Supplementary Information.

#### 4.3. Catalytic Activity Tests

The CO-PROX performance of the catalysts was evaluated at atmospheric pressure employing a continuous fixed-bed reactor. In all cases, 0.10 g of the catalyst was loaded in the quartz reactor. It was brought into contact with a feed at a flow rate of 100 mL/min. The detailed procedures for the catalytic activity tests are described in the Supplementary Information.

### 5. Conclusions

We investigated the influence of the catalyst reduction method on the CO-PROX performance of  $\text{Au}/\text{La}_2\text{O}_3/\text{Al}_2\text{O}_3$  catalysts. Aliquots of the same batch catalyst were reduced either with hydrogen by a conventional thermal method, or with  $\text{NaBH}_4$  or glycerol by a chemical method. All chemically-reduced catalysts exhibited XPS peaks shifted towards lower binding energies. A blue shift of the IR band corresponding to CO linearly adsorbed on low-coordinated Au sites was observed in the case of  $\text{Au}/\text{La}_2\text{O}_3/\text{Al}_2\text{O}_3$  catalysts reduced with  $\text{NaBH}_4$ . The size of the gold particles increased with the increasing amounts of  $\text{NaBH}_4$  used for the chemical reduction. Glycerol and glycerol-derived intermediates were detected in the catalyst reduced with glycerol and were considered responsible for the poor CO-PROX performance of this system. At low temperatures, lower CO conversions were obtained over  $\text{NaBH}_4$ - or glycerol-reduced  $\text{Au}/\text{La}_2\text{O}_3/\text{Al}_2\text{O}_3$  than hydrogen-reduced  $\text{Au}/\text{La}_2\text{O}_3/\text{Al}_2\text{O}_3$  catalysts; however, high CO conversions were observed over a wider temperature range in the case of the  $\text{Au}/\text{La}_2\text{O}_3/\text{Al}_2\text{O}_3$  catalyst reduced with an appropriate amount of  $\text{NaBH}_4$ . This catalyst showed the highest intensity of the IR band corresponding to CO adsorbed on negatively charged  $\text{Au}^{\delta-}$  sites in the DRIFT analysis of methanol decomposition. Therefore, it can be concluded that chemical reduction with an appropriate amount of  $\text{NaBH}_4$  enhances CO-PROX performance by improving the CO–Au interactions. However, an excessive amount of  $\text{NaBH}_4$  has an adverse effect on the catalytic activity because of the formation of large aggregates of gold particles.

**Supplementary Materials:** The following are available online at <http://www.mdpi.com/2073-4344/8/5/183/s1>: Loading of gold on  $\text{La}_2\text{O}_3/\text{Al}_2\text{O}_3$  support by the deposition–precipitation with urea method (DPU); The reduction of gold by the chemical reduction with glycerol (CRG) method; Characterization of catalysts; Catalytic activity tests; Figure S1: CO-PROX performance of  $\text{Au}/\text{La}_2\text{O}_3/\text{Al}_2\text{O}_3$  catalysts such as  $\text{Au}/\text{La}_2\text{O}_3/\text{Al}_2\text{O}_3$  (H) ( $\nabla$ ),  $\text{Au}/\text{La}_2\text{O}_3/\text{Al}_2\text{O}_3$  (S5) ( $\circ$ ),  $\text{Au}/\text{La}_2\text{O}_3/\text{Al}_2\text{O}_3$  (S35) ( $\square$ ),  $\text{Au}/\text{La}_2\text{O}_3/\text{Al}_2\text{O}_3$  (S115) ( $\star$ ), and  $\text{Au}/\text{La}_2\text{O}_3/\text{Al}_2\text{O}_3$  (G) ( $\diamond$ ); Figure S2: CO-PROX performance of  $\text{Au}/\text{La}_2\text{O}_3/\text{Al}_2\text{O}_3$  catalysts such as  $\text{Au}/\text{La}_2\text{O}_3/\text{Al}_2\text{O}_3$  (S35) without reduction under  $\text{H}_2$  ( $\nabla$ ) and  $\text{Au}/\text{La}_2\text{O}_3/\text{Al}_2\text{O}_3$  (G) without reduction under  $\text{H}_2$  ( $\square$ ); Figure S3: Effect of water and  $\text{CO}_2$  on the CO-PROX performance of  $\text{Au}/\text{La}_2\text{O}_3/\text{Al}_2\text{O}_3$  (S35); Figure S4: TEM images of  $\text{Au}/\text{La}_2\text{O}_3/\text{Al}_2\text{O}_3$  (S5) (a) and  $\text{Au}/\text{La}_2\text{O}_3/\text{Al}_2\text{O}_3$  (S115) (b); Figure S5: XRD patterns of  $\text{Al}_2\text{O}_3$  (a) and  $\text{La}_2\text{O}_3/\text{Al}_2\text{O}_3$  (b); Figure S6: FT-IR spectra of the as prepared  $\text{Au}/\text{La}_2\text{O}_3/\text{Al}_2\text{O}_3$  (G) sample.

**Author Contributions:** P.L. and E.D.P. conceived and designed the experiments; P.L. performed the experiments; P.L. and E.D.P. analyzed the data; P.L. and E.D.P. wrote the paper.

**Acknowledgments:** This work was supported by the Basic Science Research Program through the National Research Foundation of Korea (NRF), funded by the Ministry of Science and Information and Communication Technology (ICT, grant No. 2017R1A2B3011316).

**Conflicts of Interest:** The authors declare no conflict of interest.

## References

1. Park, E.D.; Lee, D.; Lee, H.C. Recent progress in selective CO removal in a H<sub>2</sub>-rich stream. *Catal. Today* **2009**, *139*, 280–290. [[CrossRef](#)]
2. Liu, K.; Wang, A.; Zhang, T. Recent advances in preferential oxidation of CO Reaction over platinum group metal catalysts. *ACS Catal.* **2012**, *2*, 1165–1178. [[CrossRef](#)]
3. Torres Sanchez, R.M.; Ueda, A.; Tanaka, K.; Haruta, M. Selective oxidation of CO in hydrogen over gold supported on manganese oxides. *J. Catal.* **1997**, *168*, 125–127. [[CrossRef](#)]
4. Okumura, M.; Nakamura, S.; Tsubota, S.; Nakamura, T.; Azuma, M.; Haruta, M. Chemical vapor deposition of gold on Al<sub>2</sub>O<sub>3</sub>, SiO<sub>2</sub>, and TiO<sub>2</sub> for the oxidation of CO and of H<sub>2</sub>. *Catal. Lett.* **1998**, *51*, 53–58. [[CrossRef](#)]
5. Bond, G.C.; Thompson, D.T. Catalysis by gold. *Catal. Rev. Sci. Eng.* **1999**, *41*, 319–388. [[CrossRef](#)]
6. Ko, E.Y.; Park, E.D.; Seo, K.W.; Lee, H.C.; Lee, D.; Kim, S. A comparative study of catalysts for the preferential CO oxidation in excess hydrogen. *Catal. Today* **2006**, *116*, 377–383. [[CrossRef](#)]
7. Kandai, S.; Gokhale, A.A.; Grabow, L.C.; Dumesic, J.A.; Mavrikakis, M. Why Au and Cu are more selective than Pt for preferential oxidation of CO at low temperature. *Catal. Lett.* **2004**, *93*, 93–100. [[CrossRef](#)]
8. Bond, G.C.; Louis, C.; Thompson, D.T. *Catalysis by Gold*; Imperial College Press: London, UK, 2006.
9. Mohr, C.; Hofmeister, H.; Claus, P. The influence of real structure of gold catalysts in the partial hydrogenation of acrolein. *J. Catal.* **2003**, *213*, 86–94. [[CrossRef](#)]
10. Zanella, R.; Louis, C.; Giorgio, S.; Touroude, R. Crotonaldehyde hydrogenation by gold supported on TiO<sub>2</sub>: Structure sensitivity and mechanism. *J. Catal.* **2004**, *223*, 328–339. [[CrossRef](#)]
11. Lakshmanan, P.; Park, J.E.; Park, E.D. Recent advances in preferential oxidation of CO in H<sub>2</sub> over gold catalysts. *Catal. Surv. Asia* **2014**, *18*, 75–88. [[CrossRef](#)]
12. Grisel, R.J.H.; Nieuwenhuys, B.E. Selective oxidation of CO, over supported Au catalysts. *J. Catal.* **2001**, *199*, 48–59. [[CrossRef](#)]
13. Liotta, L.F.; Di Carlo, G.; Pantaleo, G.; Venezia, A.M. Supported gold catalysts for CO oxidation and preferential oxidation of CO in H<sub>2</sub> stream: Support effect. *Catal. Today* **2010**, *158*, 56–62. [[CrossRef](#)]
14. Quinet, E.; Morfin, F.; Diehl, F.; Avenier, P.; Caps, V.; Rousset, J.L. Hydrogen effect on the preferential oxidation of carbon monoxide over alumina-supported gold nanoparticles. *Appl. Catal. B* **2008**, *80*, 195–201. [[CrossRef](#)]
15. Bethke, G.K.; Kung, H.H. Selective CO oxidation in a hydrogen-rich stream over Au/ $\gamma$ -Al<sub>2</sub>O<sub>3</sub> catalysts. *Appl. Catal. A* **2000**, *194*, 43–53. [[CrossRef](#)]
16. Quinet, E.; Piccolo, L.; Morfin, F.; Avenier, P.; Diehl, F.; Caps, V.; Rousset, J.L. On the mechanism of hydrogen-promoted gold-catalyzed CO oxidation. *J. Catal.* **2009**, *268*, 384–389. [[CrossRef](#)]
17. Stakheev, A.Y.; Kustov, L.M. Effects of the support on the morphology and electronic properties of supported metal clusters: Modern concepts and progress in 1990s. *Appl. Catal. A* **1999**, *188*, 3–35. [[CrossRef](#)]
18. Mojet, B.L.; Miller, J.T.; Ramaker, D.E.; Koningsberger, D.C. A new model describing the metal–support interaction in noble metal catalysts. *J. Catal.* **1999**, *186*, 373–386. [[CrossRef](#)]
19. Trueba, M.; Trasatti, S.P.  $\gamma$ -Alumina as a support for catalysts: A review of fundamental aspects. *Eur. J. Inorg. Chem.* **2005**, *17*, 3393–3403. [[CrossRef](#)]
20. Boronat, M.; Illas, F.; Corma, A. Active sites for H<sub>2</sub> adsorption and activation in Au/TiO<sub>2</sub> and the role of the support. *J. Phys. Chem. A* **2009**, *113*, 3750. [[CrossRef](#)] [[PubMed](#)]
21. Lin, Q.Q.; Qiao, B.; Huang, Y.; Li, L.; Lin, J.; Liu, X.Y.; Wang, A.; Li, W.C.; Zhang, T. La-doped Al<sub>2</sub>O<sub>3</sub> supported Au nanoparticles: highly active and selective catalysts for PROX under PEMFC operation conditions. *Chem. Commun.* **2014**, *50*, 2721–2725. [[CrossRef](#)] [[PubMed](#)]
22. Lakshmanan, P.; Park, J.E.; Kim, B.; Park, E.D. Preferential oxidation of CO in a hydrogen-rich stream over Au/MO<sub>x</sub>/Al<sub>2</sub>O<sub>3</sub> (M=La, Ce, and Mg) catalysts. *Catal. Today* **2016**, *265*, 19–26. [[CrossRef](#)]

23. Hugon, A.; El Kolli, N.; Louis, C. Advances in the preparation of supported gold catalysts: Mechanism of deposition, simplification of the procedures and relevance of the elimination of chlorine. *J. Catal.* **2010**, *274*, 239–250. [[CrossRef](#)]
24. Lakshmanan, P.; Upare, P.P.; Le, N.T.; Hwang, Y.K.; Hwang, D.W.; Lee, U.H.; Kim, H.R.; Chang, J.S. Facile synthesis of CeO<sub>2</sub>-supported gold nanoparticle catalysts for selective oxidation of glycerol into lactic acid. *Appl. Catal. A* **2013**, *468*, 260–268. [[CrossRef](#)]
25. Grunwaldt, J.D.; Maciejewski, M.; Becker, O.S.; Fabrizioli, P.; Baiker, A. Comparative study of Au/TiO<sub>2</sub> and Au/ZrO<sub>2</sub> catalysts for low temperature CO Oxidation. *J. Catal.* **1999**, *186*, 458–469. [[CrossRef](#)]
26. Centeno, M.A.; Paulis, M.; Montes, M.; Odriozola, J.A. Catalytic combustion of volatile organic compounds on Au/CeO<sub>2</sub>/Al<sub>2</sub>O<sub>3</sub> and Au/Al<sub>2</sub>O<sub>3</sub> catalysts. *Appl. Catal. A* **2002**, *234*, 65–78. [[CrossRef](#)]
27. Ilieva, L.; Pantaleo, G.; Sobczak, J.W.; Ivanov, I.; Venezia, A.M.; Andreeva, D. NO reduction by CO in the presence of water over gold supported catalysts on CeO<sub>2</sub>-Al<sub>2</sub>O<sub>3</sub> mixed support, prepared by mechanochemical activation. *Appl. Catal. B* **2007**, *76*, 107–114. [[CrossRef](#)]
28. Delannoy, L.; Fajerwerg, K.; Lakshmanan, P.; Potvin, C.; Methivier, C.; Louis, C. Supported gold catalysts for the decomposition of VOC: Total oxidation of propene in low concentration as model reaction. *Appl. Catal. B* **2010**, *94*, 117–124. [[CrossRef](#)]
29. Boccuzzi, F.; Chiorino, A.; Manzoli, M. FTIR study of the electronic effects of CO adsorbed on gold nanoparticles supported on titania. *Surf. Sci.* **2000**, *454*, 942–946. [[CrossRef](#)]
30. Hadjiivanov, K.J.; Vayssilov, G.N. *Advances in Catalysis*; Academic Press: New York, NY, USA, 2002.
31. Haruta, M.; Tsubota, S.; Kobayashi, T.; Kageyama, H.; Genet, M.J.; Delmon, B. Low-temperature oxidation of CO over gold supported on TiO<sub>2</sub>, α-Fe<sub>2</sub>O<sub>3</sub>, and Co<sub>3</sub>O<sub>4</sub>. *J. Catal.* **1993**, *144*, 175–192. [[CrossRef](#)]
32. Boccuzzi, F.; Chiorino, A.; Manzoli, M.; Andreeva, D.; Tabakova, T. FTIR study of the low-temperature water–gas shift reaction on Au/Fe<sub>2</sub>O<sub>3</sub> and Au/TiO<sub>2</sub> Catalysts. *J. Catal.* **1999**, *188*, 176–185. [[CrossRef](#)]
33. Frank, B.; Jentoft, F.C.; Soerijanto, H.; Kröhnert, J.; Schlögl, R.; Schomäcker, R. Steam reforming of methanol over copper-containing catalysts: Influence of support material on microkinetics. *J. Catal.* **2007**, *246*, 177–192. [[CrossRef](#)]
34. Matter, P.H.; Ozkan, U.S. Effect of pretreatment conditions on Cu/Zn/Zr-based catalysts for the steam reforming of methanol to H<sub>2</sub>. *J. Catal.* **2005**, *234*, 463–475. [[CrossRef](#)]
35. Jacobs, G.; Davis, B.H. In situ DRIFTS investigation of the steam reforming of methanol over Pt/ceria. *Appl. Catal. A. Gen.* **2005**, *285*, 43–49. [[CrossRef](#)]
36. Binet, C.; Daturi, M.; Lavalley, J.C. IR study of polycrystalline ceria properties in oxidised and reduced states. *Catal. Today* **1999**, *50*, 207–225. [[CrossRef](#)]
37. Tabakova, T.; Boccuzzi, F.; Manzoli, M.; Andreeva, D. FTIR study of low-temperature water-gas shift reaction on gold/ceria catalyst. *Appl. Catal. A* **2003**, *252*, 385. [[CrossRef](#)]
38. Date, M.; Imai, H.; Tsubota, S.; Haruta, M. In situ measurements under flow condition of the CO oxidation over supported gold nanoparticles. *Catal. Today* **2007**, *122*, 222–225. [[CrossRef](#)]
39. Wu, N.; Fu, L.; Su, M.; Aslam, M.; Chun Wong, K.; Dravid, V.P. Interaction of Fatty Acid Monolayers with Cobalt Nanoparticles. *Nano Lett.* **2004**, *4*, 383–386. [[CrossRef](#)]
40. Nor Hidawati, E.; Mimi Sakinah, A.M. Treatment of glycerin pitch from biodiesel production. *Int. J. Chem. Environ. Eng.* **2011**, *2*, 309–313.
41. Kubelkova, L.; Cejka, J.; Novakova, J. Surface reactivity of ZSM-5 zeolites in interaction with ketones at ambient temperature (a FT-i.r. study). *Zeolites* **1991**, *11*, 48–53. [[CrossRef](#)]
42. Yoda, E.; Ootawa, A. Dehydration of glycerol on H-MFI zeolite investigated by FT-IR. *Appl. Catal. A* **2009**, *360*, 66–70. [[CrossRef](#)]
43. Chan-Thaw, C.E.; Campisi, S.; Wang, D.; Prati, L.; Villa, A. Selective oxidation of raw glycerol using supported AuPd nanoparticles. *Catalysts* **2015**, *5*, 131–144. [[CrossRef](#)]

